Rock Mechanics and Rock Engineering (2019) 52:4979–4996
https://doi.org/10.1007/s00603-019-02011-3

ORIGINAL PAPER

Effect of Shear Stresses on Pillar Stability: A Back Analysis of the Troy Mine Experience to Predict Pillar Performance at Montanore Mine

T. Garza-Cruz[1] · M. Pierce[2] · M. Board[3]

Received: 31 October 2018 / Accepted: 21 October 2019 / Published online: 19 November 2019

Abstract

This paper describes the results of a back analysis of pillar failures at Troy Mine, Montana, and the use of this experience to make forward predictions on pillar stability in the nearby Montanore deposit which lies in a similar geomechanical setting. At Troy Mine, a progression of pillar failures in areas within the Middle Quartzite of the Revett formation led to the observed surface subsidence. The Troy Mine experience was used to understand the level of stresses and failure mechanism leading to the collapse of some pillars in the North Orebody to estimate pillar strength in quartzite beds within Troy's mountainous terrain. The model elucidated that the dipping orebody geometry in relation to topography led to shear stresses in pillars at Troy Mine. Shear stresses resulted in significant loss of confinement in pillar cores (many theoretically in tension), even at width-to-height ratios that would be deemed stable under zero shear stress (flat seam under flat topography). A calibrated model was achieved, which allowed us to evaluate the impact that different pillar geometric characteristics (such as width, length, height, and shape) have on pillar performance under shear conditions for different depths and extraction ratios. Design charts were then generated to provide guidance on pillar geometry based on expected demand. Mine-wide models were developed to predict the level of vertical stress and horizontal shear stress for pillars in the different ore-bearing beds at Montanore. A sensitivity study was performed for various conditions, including extraction ratio, spatial location under the mountainous terrain, and local orebody geometry with the aim of performing a mine-wide evaluation of the factor of safety against shear. The results of the analyses performed in the present work show that the use of design methods that do not take the effect of shear stresses into account may result in under-designed pillars, while a false impression of rock mass strength could be derived from back analysis.

Keywords Pillars in shear · Pillar stability · Troy mine · Montanore · Pillars in dipping seams · Pillar strength

1 Introduction

The Montanore prospect in northwest Montana is currently in the permitting process. The property has bedded copper–silver deposits dipping at an approximate average angle of 17° and is in the same quartzite beds (the Revett formation) as the now-closed Troy Mine. The mineralization is disseminated through multiple undulating beds (up to 3) that range in thickness from 5 to 15 m (16–49 ft) and are separated by a variable-thickness interbed. It is intended to mine all beds by employing a room and pillar method (heading and bench). The depth of mining varies from approximately 300 to 1000 m (954–3280 ft). The beds are located beneath rugged, mountainous terrain.

The consistency of the Revett formation is regional, stretching for tens of miles from Missoula, Montana to Coeur d'Alene, Idaho (Boleneus et al. 2006). Both the Troy and Montanore deposits are strata-bound sediment-hosted silver–copper deposits in the Revett Formation (Tetra Tech, Inc. and R Squared Incorporated 2006). Since the Montanore property lies in a similar geological and geomechanical setting as Troy Mine (Boleneus et al. 2006; FS and MDEQ 2001), it is important to use the experience acquired at this site to inform the design at Montanore. At Troy Mine, a progression of pillar failures in late 2012 and early 2013 in areas within the Middle Revett led to surface subsidence. In

✉ T. Garza-Cruz
tgarza@itascacg.com

[1] Itasca Consulting Group, Inc, Minneapolis, MN, USA

[2] Pierce Engineering, Minneapolis, MN, USA

[3] Hecla Mining Company, Coeur d'Alene, ID, USA

addition, some hour-glassing of pillars has been reported, especially in over-stressed areas.

The Troy Mine experience was used to understand the level of stresses and failure mechanism leading to the collapse of some pillars in the North Orebody to estimate pillar strength in quartzite beds within Troy's mountainous terrain. A calibrated model was achieved, which allowed us to evaluate the impact that different pillar geometric characteristics (such as width, length, height, and shape) have on pillar performance under shear conditions for different depths and extraction ratios. This analysis was then used to generate site-specific design charts to provide guidance on pillar geometry based on expected demand. Mine-wide models were developed to understand the level of vertical stress and horizontal shear stress that pillars in the different beds at Montanore would be subject to depending on extraction ratio, spatial location under the mountainous terrain, and local orebody geometry. The aim was to provide recommendations on pillar geometry and extraction ratios to feed into the Montanore Mine design.

2 Background and Key Assumptions

The Spar Lake deposit (Troy Mine) and Rock Lake deposit (Rock Creek and Montanore deposits) are located beneath rugged terrain in the Cabinet Mountains of northwest Montana. The Troy Mine is located 14 miles (23 km) south of Troy, Montana in Lincoln County. The Montanore deposit is located approximately 20 miles (32 km) south of Libby, Montana and 9 miles (14.5 km) northeast of Noxon, Montana. The Montanore property lies in a similar geological and geomechanical setting as Troy Mine (Boleneus et al. 2006; FS and MDEQ 2001), which is located about 30 miles (48 km) away.

The Revett Formation is over 600 m (1969 ft) thick and is divided into lower, middle, and upper members that consist of interbedded metamorphosed sandstones, siltstone, and shale (Hayes 1983). All three members are recognizable at the Troy Mine (Bowden 1977; Hayes 1983). In the Troy Mine area, the formation is mainly biotite-grade quartzite, siltite, and argillite beds. The Upper and Lower Revett members contain thick units of well-indurated quartzitic sandstones, which host the majority of the copper and silver mineralization (Hayes 1983; Boleneus et al. 2006). The Middle Revett Member is mainly siltite and argillite. Folding and thrust faulting have deformed the mineralized zones, and they have been further segmented by high-angle faulting. Faults associated with the deposits include the East and Cross Faults at the Troy Mine, and the Rock Lake and Libby Lake Faults at Montanore. Although there are structural differences between the two properties, the mineralogy of the ore zones is essentially the same (FS and MDEQ 2001). Figure 1 shows the generalized stratigraphic columns of the Revett Formation at the Troy Mine and Rock Creek-Montanore deposits (Boleneus et al. 2006).

It is important to note that while most of the mining at Troy was focused on the middle quartzite in the Upper Revett (although some mining occurred in the A-Bed and C-Bed in the Upper Revett), the Montanore project would be mainly targeting the upper portion of the Lower Revett. Both the Troy Mine and Montanore deposit are located under mountainous terrain, as shown in Figs. 2 and 3.

There is limited information available on rock strength of the Revett formation specifically at the Montanore site, but there are available data from mining in the same geologic units in the prolific Coeur d'Alene mining district located less than 100 km away to the southwest. The compressive strength, tensile strength, and elastic properties of the three rock types defined within the Lower Revett (quartzite, silty quartzite, and siltite) are listed in Table 1 (Noranda and Call and Nicholas 1989). The data show that as the silt content increases, the uniaxial compressive strength decreases. As a first approximation, the contact strength of the bonded block models presented here is based on the properties of the Silty quartzite.

The Lower Revett has a mean bedding plane spacing of 1.1 m (3.6 ft) (Noranda and Call and Nicholas 1989); this bedding spacing is used in subsequent analyses presented here. For reference, Troy Mine is located in the upper Revett quartzite, which is characterized by very strong intact rock, with continuous bedding planes parallel to the dip of the unit as well as closely spaced cross jointing. The spacing of the through-going beds is of the order of 1 m (3–4 ft), and some of the beds have relatively thick clay on their surfaces.

There are no in situ stress measurements available at either Montanore or Troy mine. In situ stress data from Coeur d'Alene, which is also in the Belt Series, lists the horizontal stress ranging from 1.2 to 1.9 times the vertical stress (Noranda and Call and Nicholas 1989), while others report a maximum-to-minimum horizontal stress of approximately 1.4 (Langstaff 1976; Beus and Chan 1980; Board and Beus 1989).

2.1 Key Assumptions

Initially, it was assumed that the middle quartzite in the Upper Revett (Troy) and the Lower Revett (Montanore) formations were similar; hence, it was deemed appropriate to back analyze Troy and use the calibrated rock mass properties to evaluate the Montanore design.

After a re-visitation of the available core from Montanore was done by Hecla personnel (Board 2017), it was noted that the breaks in the Lower Revett core are clean and unaltered, and do not exhibit clay infill in the bedding planes as the quartzite at Troy (Upper Revett), suggesting that the rock

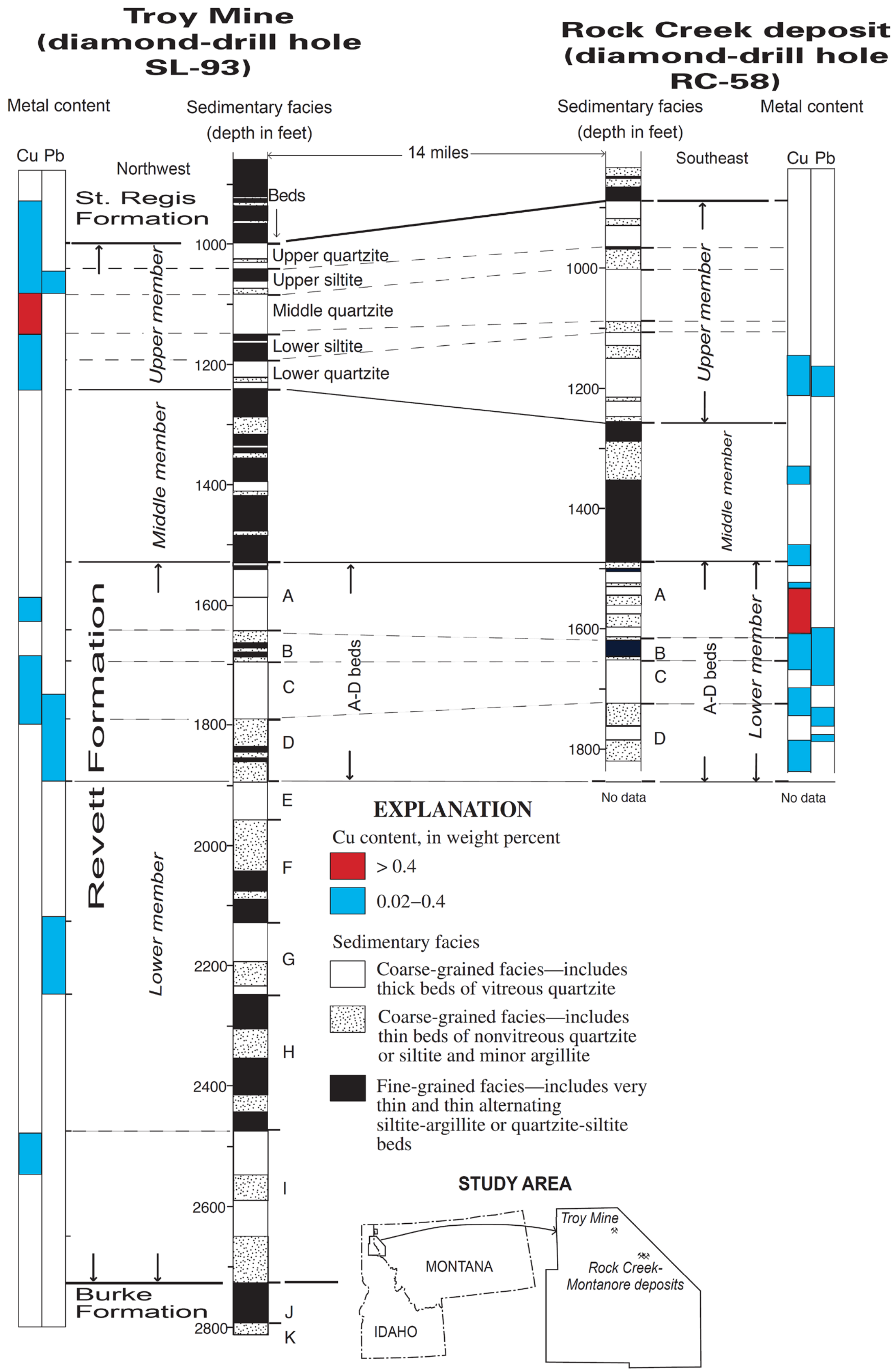

Fig. 1 Generalized stratigraphic columns of the Revett Formation at the Troy Mine and Rock Creek-Montanore deposits, western Montana (Boleneus et al. 2006)

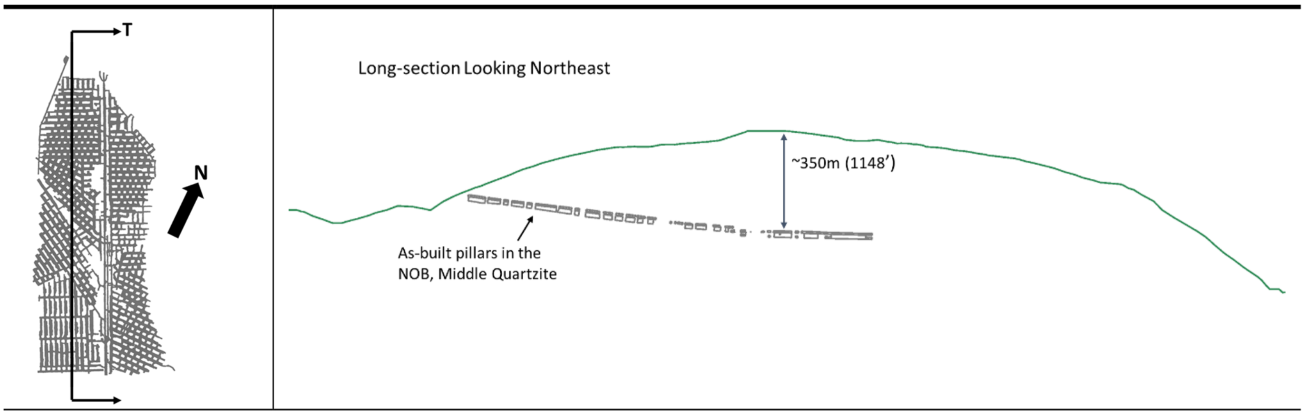

Fig. 2 Spatial location of the North Orebody as-built pillars in the Middle Quartzite at Troy with respect to topography (green) through cross section T

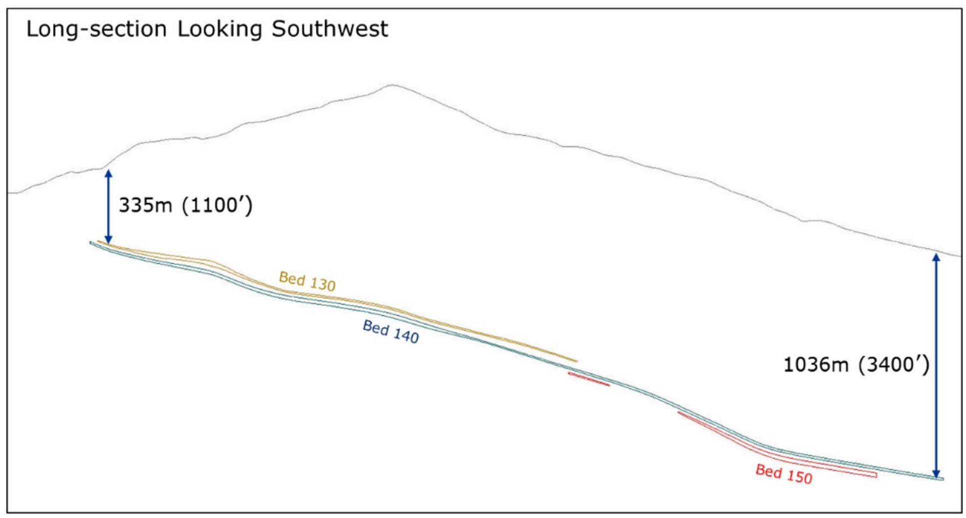

Fig. 3 Deposit geometry at Montanore relative to topography

Table 1 Summary of rock mechanical properties—lower Revett formation (Noranda, Call and Nicholas 1989)

	Uniaxial compressive strength		Tensile strength		Young's modulus		Poisson's ratio
	(MPa)	(psi)	(MPa)	(psi)	(MPa)	(psi)	
Quartzite	368	53,302	15	2202	46953	6.81E+06	0.22
Silty quartzite	177	25,709	14	1964	57,158	8.29E+06	0.22
Siltite	151	21,918	–	–	57,709	8.37E+06	0.24

mass strength of the Lower Revett is likely to be higher than that of the Upper Revett. A rock mass characterization campaign is warranted to reduce the uncertainty going forward.

At this point, it became evident that while the intact rock at Troy is stronger than at Montanore (Troy is mostly quartzite, while siltite content is higher at Montanore), and the bedding and joint spacing is similar at both locations, some of the beds at Troy have relatively thick clay on their surface, which is absent at Montanore. As it will be shown later in this paper, the strength of a pillar under shear conditions is sensitive to the assumed contact friction angle. It is not clear how the different combinations of intact rock strength and weaker or stronger structures counteract each other; hence, further analysis taking into account the differences between the two sites as more data becomes available is warranted.

3 Troy Mine Back Analysis

A large-scale, elastic, three-dimensional FLAC3D (Itasca 2017) model incorporating topography, orebody geometry, and as-built pillar geometries in the Middle Quartzite of the North Orebody at Troy mine was constructed. The objective of this analysis was to use the Troy Mine experience to understand the level of stresses and failure mechanism leading to the collapse of some pillars to estimate pillar strength in quartzite beds within Troy's mountainous terrain.

The model specifically targeted a number of pillars that failed in the northwest part of the North Orebody in the Middle Quartzite at Troy (see Fig. 4). In this area, the pillars were roughly square in plan with width and length of approximately 13.7 m (55 ft) and heights of approximately 23 m (75 ft). The extraction ratio in this area was 75%. These dimensions were used in the back analysis of pillar strength.

Because in situ stress measurements at Troy are not available, two different in situ stress regimes ($K0=1$ and $K0=2$) were assumed. These were based on previous assumptions of in situ stress for Troy Mine as well as data from the Coeur d'Alene, which is also in the Belt Series, listing the horizontal stress ranging from 1.2 to 1.9 times the vertical stress (Noranda and Call and Nicholas 1989).

After a hydrostatic stress state was initialized, the model was run until mechanical equilibrium was achieved. At this point, the local orientation of the stress tensors naturally rotates, aligning to the surface topography. After initial equilibrium but before mining, lateral stresses were increased in each zone to reflect low ($K0=1$) or high ($K0=2$) horizontal stress regimes and the model was run until mechanical equilibrium was achieved. It is important to note that the imposed lateral stress values are not necessarily horizontal, but they honor the local orientation of the stress tensor after initial equilibrium (following the topography near surface). This is illustrated in Fig. 5, where the pre-mining stress tensors on a vertical section along dip of the North Orebody are shown (mined geometry shown to aid visualization). This is important, because the orebody geometry in relation to the topography can lead to significant shear stresses in the pillars.

The model was excavated honoring the as-built pillar geometries in the North Orebody at Troy and run until mechanical equilibrium was achieved. After mining, every pillar was analyzed in terms of σ1, σ3, and shear

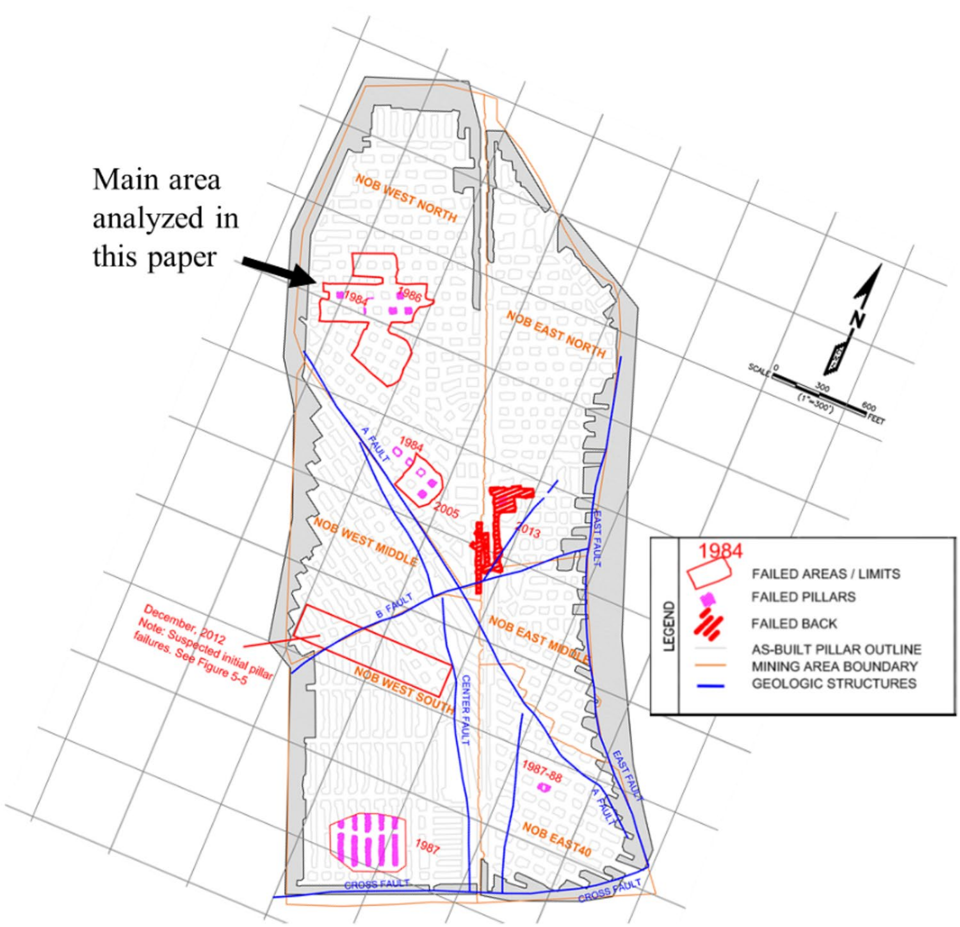

Fig. 4 Observed pillar failures in the north orebody of the middle quartzite at Troy Mine Modified after Cicchini and Killian (2014). Pillar failure in the northwest is analyzed in this paper

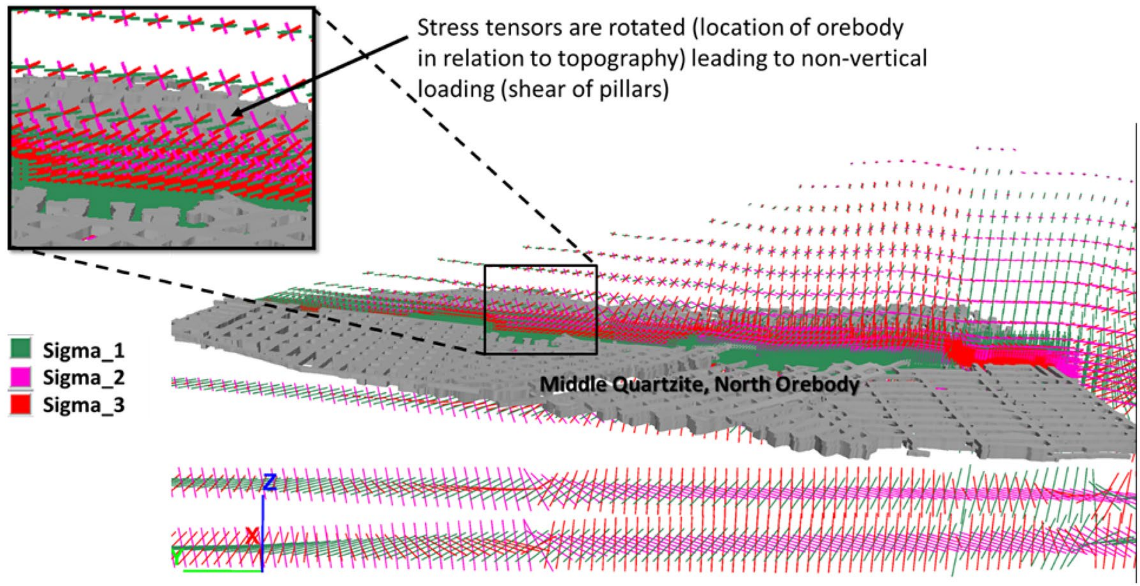

Fig. 5 Pre-mining stress tensor on vertical section along dip of the North Orebody in the Middle Quartzite at Troy. The mined geometry is shown in gray to aid visualization

stresses, averaged over the pillar and also in the pillar core.

By comparing model results with actual pillar collapses in the Middle Quartzite at Troy, a pillar average $\sigma 1 = 17–20$ MPa (2466–2900 psi) appears sufficient to cause pillar failure when pillar core confinement is very low. This is approximately 10–11% of the intact UCS and is considered reasonable when the presence of persistent bedding planes and also cross jointing is considered. For comparison, limestone pillars typically start spalling when average stress is 11–12% of lab UCS (Esterhuizen et al. 2008).

The model elucidated that the orebody geometry in relation to topography led to significant shear stresses in pillars at Troy Mine. Shear stresses resulted in significant loss of confinement in pillar cores (many theoretically in tension), even at W:H ratios that would be deemed stable under zero shear stress (flat seam under flat topography). In general, the pillars in the northwest region (see Fig. 4) were subjected to a $\sigma 1$ stress of approximately 17–20 MPa (2466–2900 psi), with a horizontal shear stress (maximum shear stress resolved in a horizontal plane at the mid-height of the pillar) of approximately 3 MPa (435 psi) for the $K0 = 1$ case and 4 MPa (580 psi) for the $K0 = 2$ case.

The detrimental effect of shear stresses on the stability of pillars in orebodies in shear has been identified by others (Hoek and Brown 1980; Coates 1981; Pariseau 1982; Suorineni et al. 2011; Mgumbwa 2011; Suorineni et al. 2014).

4 Pillar Model Calibration to the Troy Conditions

A calibration exercise was launched to match the pillar performance under the stress conditions present at Troy. A bonded block model (BBM) was assembled with bond strengths informed by a distribution of tensile strength of the Lower Revett Silty Quartzite to represent the rock mass. Explicit bedding planes were incorporated, and non-persistent cross joints were systematically introduced. The aim was to perform a calibration exercise informed by the Lower Revett strengths to match Troy pillar conditions under the stress state present, assuming that quartzites found in the Upper (Troy) and Lower Revett (Montanore) formations are similar. Once the model properties are calibrated to match observations, a series of site-specific design charts were developed to evaluate pillar performance in a mine-wide design.

4.1 Bonded Block Model

3DEC (Itasca 2016a) was used to represent the rock mass as a collection of interlocked tetrahedral blocks bonded at their contacts to simulate a pillar under the Troy stress conditions. 3DEC was selected, as it can be used to simulate a rock mass as bonded polyhedral elements (tetrahedral in this case) that can break at their subcontacts as a result of stress concentrations, mimicking the initiation of cracks that can coalesce and/or propagate to fracture the rock mass. This results in an emergent damage pattern with associated bulking. The 3DEC approach differs from particle-based methods such as PFC3D (Itasca 2014) in its ability to represent a zero initial porosity condition, as well as interlocked irregular block shapes that provides resistance to block rotation (moments) after contact breakage. These processes tend to dominate the rock mass behavior in low confinement zones near excavations (Kaiser 2016).

While discontinuum approaches such as the Discrete Element Method (DEM) have been shown to realistically simulate the initiation, propagation, and coalescence of cracks leading to face-parallel fracturing (spalling), as well as the rock mass strength dependency on confinement (Damjanac et al. 2007; Lan et al. 2010; Garza-Cruz et al. 2014), these DEM models are still computationally expensive. It is important to mention that the Bonded Block Model is intended to provide enough pathways in 3D to allow the synthetic rock to develop fractures that would be representative of the fracturing that would occur in a typical excavation through the rock mass of interest. It is not meant to represent the fracturing occurring at the grain level. In a BBM, the fracturing would follow the minimum energy requirement path, with a more "jagged" response with larger block size, while smaller block sizes would develop a somewhat "smoother" oscillation around the same mean path. For practical applications, a balance between run time (directly impacted by the block size modeled) and realistic behavior need to be struck, knowing that the minimum emergent fragment size is constrained by the block size selected.

A rock mass sample was constructed by assembling a collection of highly interlocked tetrahedral blocks with an approximate edge length of 2 m (6.5 ft) using Griddle (Itasca 2016b) and importing them into 3DEC. A tensile strength distribution was constructed using the results of tensile tests on the Lower Revett Silty Quartzite to inform the bond strength of a bonded block model (BBM) to represent the rock mass. The Lower Revett Silty Quartzite is characterized by a mean tensile strength of 13.5 MPa (1958 psi) with a standard deviation of 4.84 MPa (702 psi) (Noranda and Call and Nicholas 1989). To populate the BBM sample, each block contact was assigned a tensile strength value randomly selected from the cumulative distribution of rock tensile strength (see Fig. 6), and its local cohesion was set to be 2.5 times that tensile strength following the methodology described by Garza-Cruz and Pierce (2014). This cohesion-to-tensile-strength ratio was based on a sensitivity study in which such ratios produced a macro-unconfined compressive strength (UCS)/tensile strength ratio of the order of 10–15. In all models, the blocks were defined as elastic, while the contacts follow a Mohr–Coulomb constitutive model. It is important to mention that additional models of selected pillar dimensions were run using an approximate edge length of

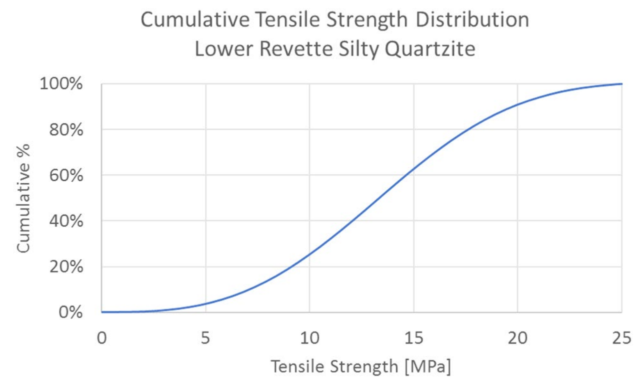

Fig. 6 Cumulative tensile strength distribution based on available data of the Lower Revett Silty Quartzite (mean tensile strength of 13.5 MPa with a standard deviation of 4.84 MPa). This is later used to populate the BBM contact properties

Table 2 Block and contact properties used in the BBM model

Block properties	
Young's modulus	50 GPa
Poisson's ratio	0.25
Density	2600 kg/m^3
Contact properties	
Normal stiffness	105 GPa/m
Shear stiffness	52.5 GPa/m
Peak friction angle	30°
Residual friction angle	30°
Dilation angle	10°
Peak tensile strength	Variable (see Fig. 6)
Residual tensile strength	0
Peak cohesive strength	2.5 × tensile strength
Residual cohesive strength	0

0.5 m (1.6 ft) instead of 2 m (6.5 ft) to evaluate the sensitivity of the emergent pillar strength to the block size selected. For the range of pillar dimensions evaluated in this work, the pillar strengths obtained using a 2 m edge length were in line with those obtained with an edge length four times smaller (0.5 m), which means that for the purpose of characterizing the strength of the pillar sizes relevant to this work, the resolution given by the block edge length selected is sufficient.

The mechanical properties of the blocks and block contacts are summarized in Table 2. Young's Modulus of the blocks was assumed to be that of the intact Quartzite (50 GPa or 7.2×10^6 psi). The presence of discontinuities contributes to a reduction of the rock mass Young's Modulus that can be estimated through rock mass quality, i.e., geological strength index (GSI). In this study, a rock mass Young's Modulus of 11 GPa or 1.6×10^6 psi was assumed and achieved through the selection of pertinent block-contact normal and shear stiffness. This rock mass Young's Modulus was calculated using Eq. (1) by assuming a $GSI=45$, and a disturbance factor $D=0$ (Hoek and Diederichs 2006). Bedding planes were explicitly represented using the cutting capabilities in 3DEC and are assumed to be horizontal, fully persistent, frictional features with a spacing of 1.1 m or 3.6 ft (Noranda and Call and Nicholas 1989), while cross-cutting joints were introduced along pre-existing polyhedral boundaries:

$$E_{\mathrm{rm}} = E_i\left(0.02 + \frac{1 - D/2}{1 + \mathrm{e}^{\left(\frac{60+15D-\mathrm{GSI}}{11}\right)}}\right). \tag{1}$$

4.2 Calibration of the BBM to the Troy Experience

The results of elastic numerical model analyses performed using the as-built geometry of the pillars in the northwest region of the Middle quartzite at Troy mine elucidated that the pillars were subjected to an average stress between 17 and 20 MPa (2466–2900 psi) with horizontal shear stresses (maximum shear stress resolved on a horizontal plane) of 3–4 MPa (435–580 psi) depending on the in situ stress assumed ($K0=1$ and $K0=2$).

A bonded block model sample was calibrated to back analyze the pillar behavior at Troy under the described conditions. Due to the uncertainty in rock mass properties, the calibration was performed by systematically introducing random non-persistent joints (changing the properties of selected contacts along pre-existing polyhedral boundaries to exhibit zero cohesion and zero tensile strength) to weaken the rock mass until a match in behavior under the Troy conditions was found. In all BBM models, the stiffness of the contacts between blocks (joints and intact rock) was assumed to be uniform, as listed in Table 2. Both the bedding planes and the jointing were modeled as purely frictional contacts.

For each of the tests performed, a BBM sample was populated and its stresses initialized to represent a volume of quartzite at 200 m (656 ft) depth under hydrostatic stress conditions. A pillar 13.7 m (45 ft) wide by 13.7 m (45 ft) long by 23 m (75 ft) high with an extraction ratio of 75% was carved from the BBM sample by slowly relaxing the reaction forces of the excavation, which is an approximation for 3D effects at the excavation face. Lateral symmetry boundary conditions were assumed, effectively representing an infinite array of pillars.

After the pillar was excavated and mechanical equilibrium achieved, it was tested under two different loading conditions (as shown in Fig. 7):

1. uniaxial loading until failure occurred to compute its maximum load capacity;
2. keeping the vertical stress condition represented constant (approximately 200 m or 656 ft depth of cover), horizontally shear the pillar until failure occurred to compute the shear stress at failure.

A friction angle of 30° was assumed between all contacts (including bedding planes and joints). The level of jointing was varied until a pillar failing under the Troy conditions was simulated. Figure 7 shows the failed pillars under the conditions tested. The different colors represent distinct fragments (collection of bonded blocks or single blocks, whose contacts with the surrounding blocks are fully broken), while the black lines represent cracks with an aperture of at least 3 mm (0.12 in).

Table 3 lists the results of the calibration exercise (labeled pessimistic case), showing that under the absence of shearing, the simulated pillar exhibited a strength of 25.5 MPa (3700 psi), and, hence, would have been deemed as stable under pure uniaxial loading conditions based on tributary area theory. However, in reality, the pillars would have been subjected to a horizontal shear stress of the order of 3–4 MPa (depending on in situ stress regime) as shown by the large-scale elastic model, which allowed the pillar to fail under the 19 MPa (2765 psi) average vertical stress. This is because horizontal shear stresses on the pillar result in significant loss of confinement in the pillar core (sometimes putting the core in tension), negatively affecting the load capacity of the pillar. An apparent factor of safety (FOS) can be calculated as the ratio between the pillar vertical strength in the absence of shearing and the average pillar vertical stress demand, suggesting an apparent FOS = 1.34. This is the FOS that would have been estimated if the pillar existed in a flat seam under a flat surface topography. This has large implications on pillar design, since the use of design methods that do not take into account the detrimental effect of shear stresses on pillar capacity may result in under-designed pillars if they are to perform under shearing conditions. In addition, back analysis of the failed pillars without taking such shearing effect into account could also result in underestimation of the rock mass strength.

As previously mentioned, it has been noted that the breaks in the Lower Revett core are clean and unaltered, and do not exhibit clay infill in the bedding planes as in the quartzite at Troy (Upper Revett). Therefore, it was concluded that the rock mass strength of the Lower Revett could be higher than that of the Upper Revett. At this point, it became evident that while the intact rock at Troy is stronger than at Montanore (Troy is mostly quartzite, while siltite content is higher at Montanore), and the bedding and joint spacing is similar at both locations, some of the beds at Troy have relatively thick clay on their surface, which is absent at Montanore. Therefore, an additional case was run (keeping the same level of jointing) in which the contact friction angle

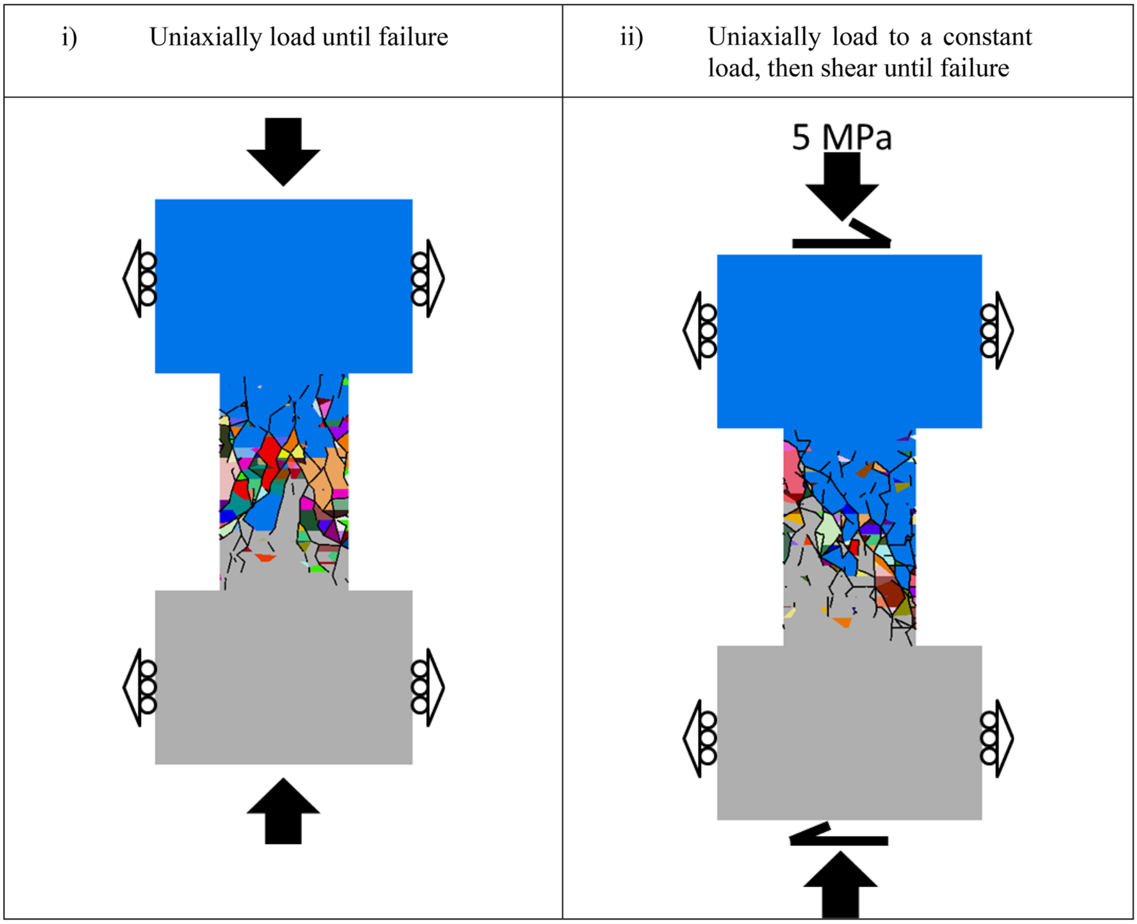

Fig. 7 Loading conditions used in calibration exercise to match Troy experience. Pillars are 13.7 m wide by 13.7 m long by 23 m high (45 by 45 by 75 ft, respectively), assuming a 75% extraction ratio. Different colors represent fragments (collection of blocks that are fully detached from their neighboring blocks) on a vertical cross section through the center of the pillar. Black lines represent cracks with normal opening of at least 3 mm (0.9 in)

Table 3 Results of the BBM pillar calibration exercise

Calibration	Pillar average vertical stress	Shear stress at failure	Pillar vertical strength (no shearing)	Apparent FOS
Pessimistic	19 MPa (2765 psi)	3.6 MPa (522 psi)	25.5 MPa (3700 psi)	1.34
Optimistic	19 MPa (2765 psi)	5.5 MPa (798 psi)	35 MPa (5076 psi)	1.84

was increased to 40° to model a more optimistic rock mass behavior that represented more frictional features (absence of clay infill) to get a range of behaviors given the uncertainties on properties and in situ stress. As noted in Table 3, the higher friction angle increases the pillar strength from 25.5 to 35 MPa (3700–5076 psi) in the absence of shear. It is not clear how the different combinations of intact rock strength and weaker or stronger structures counteract each other (Troy intact strength has been under-represented using lower intact strengths more consistent with Montanore); hence, further analysis considering the differences between the two sites as more data becomes available is warranted. Due to the absence of clay infill in bedding planes at Montanore, it was decided that the optimistic strength case is more in line with the Lower Revett than the pessimistic case calibrated. Therefore, the optimistic case was carried forward in subsequent analysis of Montanore.

As a comparison, Fig. 8 shows an empirical pillar strength for Troy of approximately 44–67 MPa (6382–9718 psi) without considering the effect of cross-jointing or bedding planes (under uniaxial loading conditions with no shear). Since the effect of shear stresses on pillars is not captured

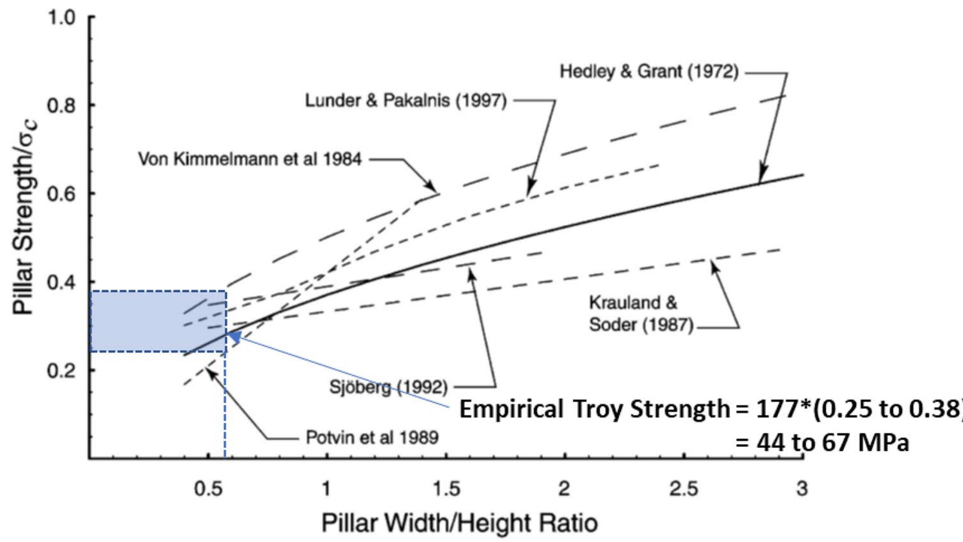

Fig. 8 Approximate Troy pillar strength based on empirical pillar strength for hard-rock pillars (modified after Martin and Maybee 2000)

on this chart, it should not be used to back analyze pillar response under shear conditions, as it would suggest that a lower rock strength, and not the loading conditions, is the main contributor to the pillar failure.

5 Impact of Pillar Geometry on Its Performance Under Shear Conditions

Pillar performance is impacted by the pillar geometric characteristics (e.g., width, length, height, and shape), extraction ratio, orebody geometry in relation with topography, as well as by the in situ stress conditions. A series of tests were performed on BBM pillars based on the optimistic calibrations described in the previous section. The objective was to test a range of pillar geometries, extraction ratios, and depths to generate site-specific design charts to provide guidance on pillar geometry based on expected demand.

Due to the inclined nature of the orebody at Montanore, it is more desirable (in terms of practical mine design) to have non-right-angled pillars in plan, such as rhomboidal-shaped pillars. To capture the pillar shape effect on its loading capacity, the hydraulic radius (HR) of the pillars tested was computed as the pillar area, divided by the pillar perimeter; while the slenderness of the pillar was calculated as the hydraulic-radius-to-height ratio (HR:h). This is important, because pillar shape affects the effective size of the confined core (due to loss of confinement near sharp corners), with rhomboidal pillars having smaller confined cores and hence lower capacity than their rectangular counterparts. Figure 9 shows a plan view of two pillars (one rhomboidal and one rectangular) with equivalent minimum width, plan area, and extraction ratio. For comparison, assume that the width of the pillar is 18 m, the length is 12 m, and the height is 16 m (59 by 39 by 52.5 ft, respectively), with the rhomboidal pillar having a 45° angle between pillar vertical sides (versus 90° for the rectangular pillar). Such a rhomboidal pillar would have an HR:h ratio of 0.19, while its rectangular counterpart would have an HR:h ratio of 0.23. Under the described geometry, the rectangular pillar would have an

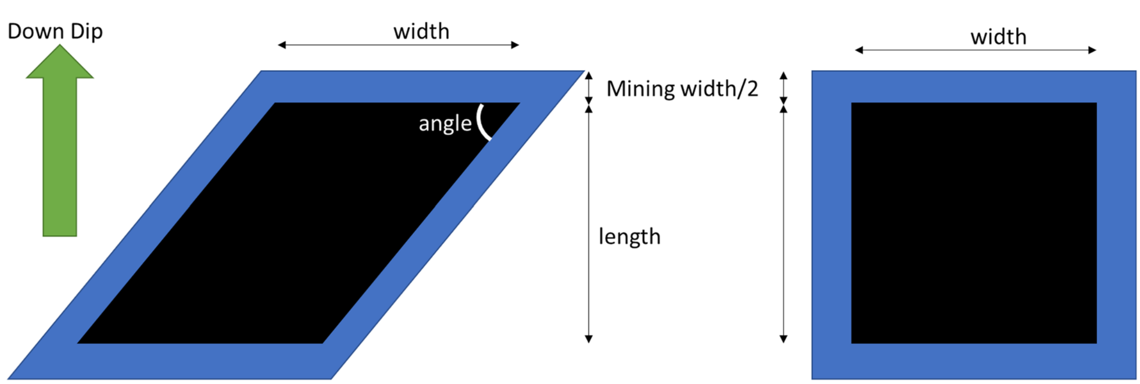

Fig. 9 Plan view of the geometric characteristics of a rhomboidal and a rectangular pillar with equivalent length, width, and area

HR:h ratio 21% larger than the rhomboidal one. This makes hydraulic radius a better measure of pillar shape than pillar width alone. In addition, by describing the pillar geometric characteristics via HR:h ratio, the load capacity of different shaped pillars can be compared on the same graph.

The pillars were first excavated under a hydrostatic stress condition ($K0 = 1$) based on a predefined depth. In all tests, 12 m (39 ft) mining widths were assumed, so different pillar hydraulic radii were tested by assuming different extraction ratios.

After excavation of the modeled BBM pillars, those that survived were horizontally sheared, keeping the vertical load constant, until failure occurred to obtain their horizontal shear strength under the vertical conditions tested. As previously noted, horizontally shearing the pillar compromises the pillar core confinement, negatively affecting the load capacity of the pillar. The results of the shear tests for the different ranges of pillar vertical stresses tested as a function of pillar HR:h ratio for the optimistic case are summarized in Fig. 10. The shear FOS indicated in the graphs was calculated as the pillar horizontal shear stress divided by the maximum horizontal shear strength for the different HR:h ratios. In general, squatter pillars are able to retain a higher level of confinement in their cores upon excavation and, hence, are able to sustain larger levels of shear under a given vertical stress. In addition, the initial level of confinement for a pillar of a given geometry also depends on the local in situ stress level before the pillar is mined; therefore, pillars with a high HR:h ratio would have a larger level of core confinement if they are located deeper in the mine. It is the interplay between pillar demand and pillar strength based on confinement that determines the emergent pillar stability. It is important to note that the factors of safety reported are based on a total loss of pillar, where the pillar core is completely compromised (FOS = 1). By this definition, pillars may still be non-serviceable at FOS > 1 (e.g., severe spalling of pillar sidewalls); therefore, a more refined approach that takes into account pre-failure serviceability is warranted for future design. These design charts are later used to evaluate the FOS of pillars in a mine-wide model based on their geometric characteristics, along with their local vertical load and shear demand.

6 Mine-Wide Pillar Stability Evaluation

A series of large-scale, elastic, three-dimensional FLAC3D models incorporating topography and orebody geometry were built to provide insight into the level of vertical stress and horizontal shear stress that pillars in different parts of the mine would experience after mining the different mineralized beds.

Because in situ stress measurements at Montanore are not available, a hydrostatic in situ stress regime ($K0 = 1$) was assumed. After the stress state was initialized, the model was run until mechanical equilibrium was achieved. As previously noted, the principal directions of the in situ stress are not aligned to vertical and horizontal planes near surface, but rather follow the topography. The orebody geometry in relation to the topography can lead to significant shear stresses in the pillars.

The Montanore deposit is approximately 760 m wide by 3960 m long (2493 by 12,992 ft, respectively). Three mining beds have been delineated at Montanore with the intention to mine them by employing a room and pillar method (heading and bench). The shape in plan of the three beds is shown in Fig. 11. The 140 bed is the most extensive and is located in the middle with the 130 bed immediately above it and the 150 bed below it. The interbed dimensions allows for a minimum thickness of 15 m (50 ft). The depth of mining varies from approximately 300–1000 m (984–3281 ft).

6.1 Pillar Stability Evaluation

Generic mine-wide pillar arrangements with a staggered pillar multi-seam configuration (see Fig. 12) were evaluated based on different extraction ratios (60, 50, and 40%), keeping the mining widths constant at 12 m (39 ft), as shown in Fig. 13. The aim is that this would allow us to get a sense for the level of vertical stress and horizontal shear stress the pillars with different characteristics would be subjected to depending on their spatial location within the mine. Table 4 lists the pillar dimensions adopted in the models based on extraction ratio. The mine-wide pillar arrangements followed the minable beds; hence, the height of each pillar varies with the local bed thickness.

The 140 bed was mined first, followed by bed 130, and finally, bed 150. Upon mining of each seam, the model was equilibrated, then the average vertical stress, horizontal shear stress, as well as the HR:h ratio was computed for each pillar. The shear FOS was computed for each of the pillars by first finding the relevant stability chart in Fig. 10 that encompassed the range of vertical stress the pillar was subjected to. On the selected chart, the shear FOS is obtained by combining the HR:h ratio (x-axis) with the pillar shear demand (y-axis). This was done automatically for each pillar by digitalizing the charts and using them as look-ups in FLAC3D to establish the local pillar shear FOS.

To evaluate the effect pillar shape has on pillar stability in different parts of the mine, the shear FOS was also calculated for pillars with equivalent width and area in plan but with rhomboidal shape (assuming angle = 45°, see Fig. 9) by calculating their corresponding HR:h ratio. As previously shown, pillar shape affects the effective size of the confined core (due to loss of confinement near sharp

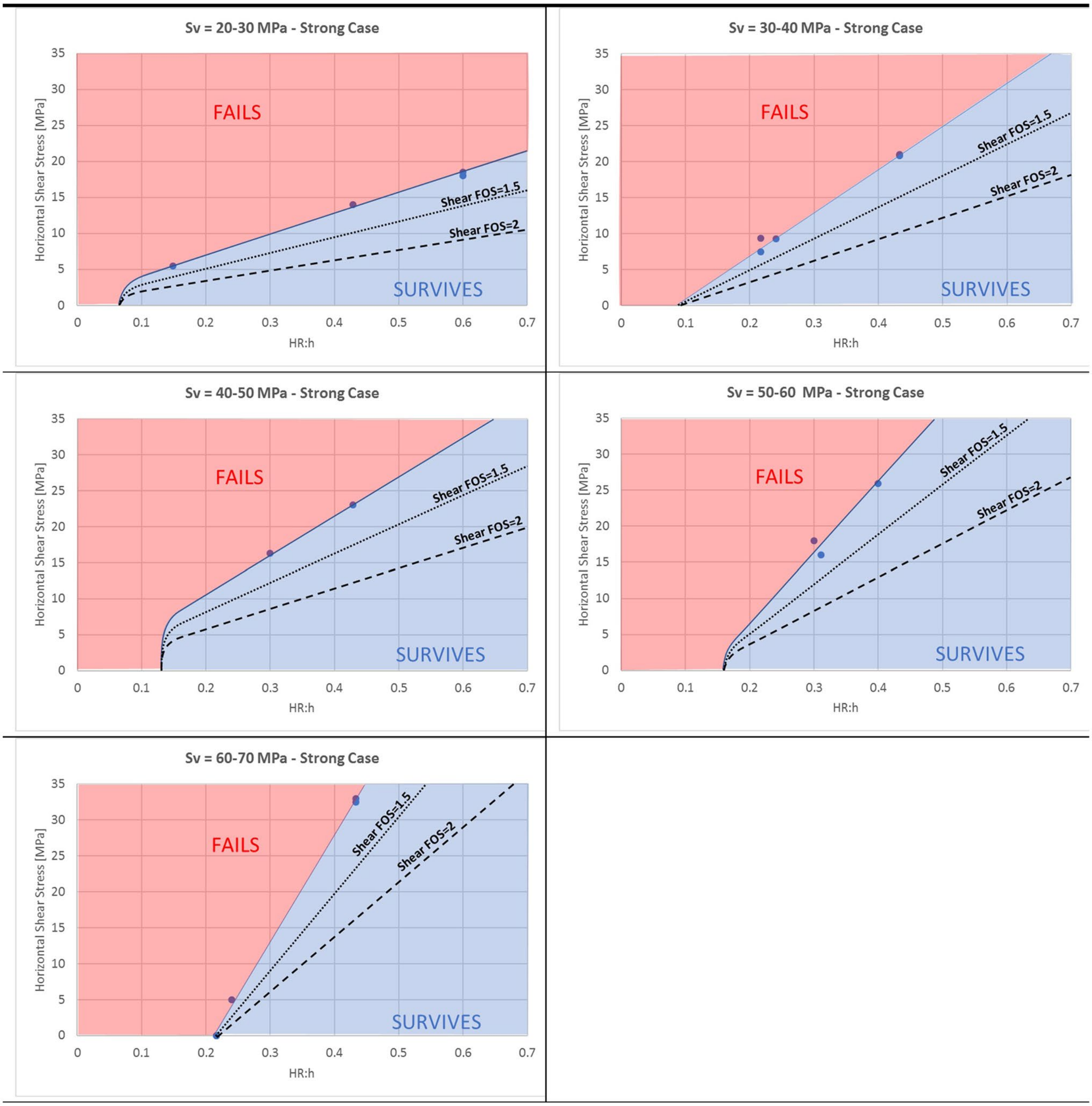

Fig. 10 Horizontal shear stress as a function of the ratio of hydraulic radius to height for different ranges of pillar average vertical stress for the optimistic case (stronger)

corners), with rhomboidal pillars having smaller confined cores and, hence, lower capacity than their rectangular counterparts, which can be quantified via HR:h ratio. The shear FOS of each pillar assuming the new HR:h ratio based on the new shape and angle was evaluated against the stability charts in Fig. 10 to compare it to their rectangular counterparts. The shear factors of safety developed in this work are based on a total loss of pillar, where the pillar core is completely compromised. Pillars may still be non-serviceable at FOS > 1 by this definition (e.g., severe spalling of pillar sidewalls).

The average vertical stress and horizontal shear stress experienced by pillars in the different beds along with their corresponding shear FOS are shown in Fig. 14 for the staggered configuration with 60% extraction ratio. The different beds are shown side by side to aid visualization. This corresponds to the stage after the three different beds have been mined. The maximum average pillar vertical stress in the

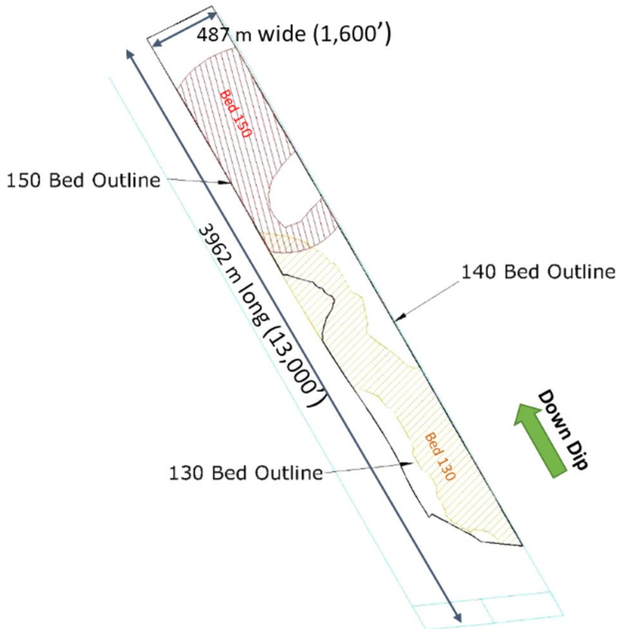

Fig. 11 Plan view of the Montanore deposit geometry

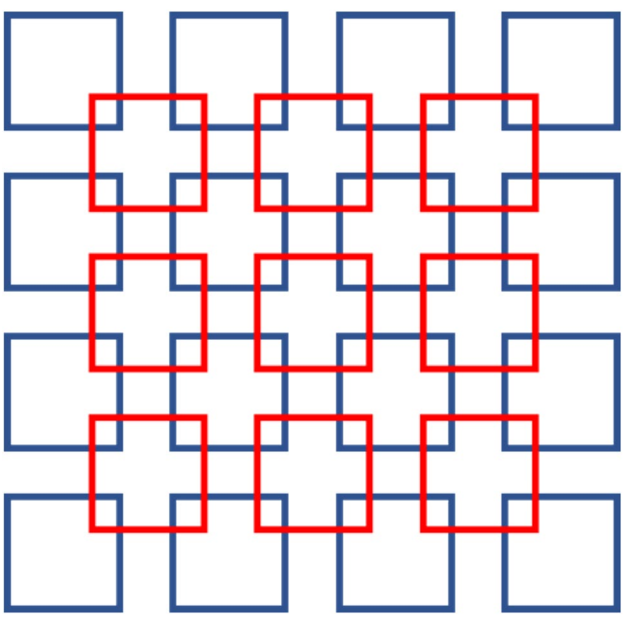

Fig. 12 Plan view of the staggered pillar configuration

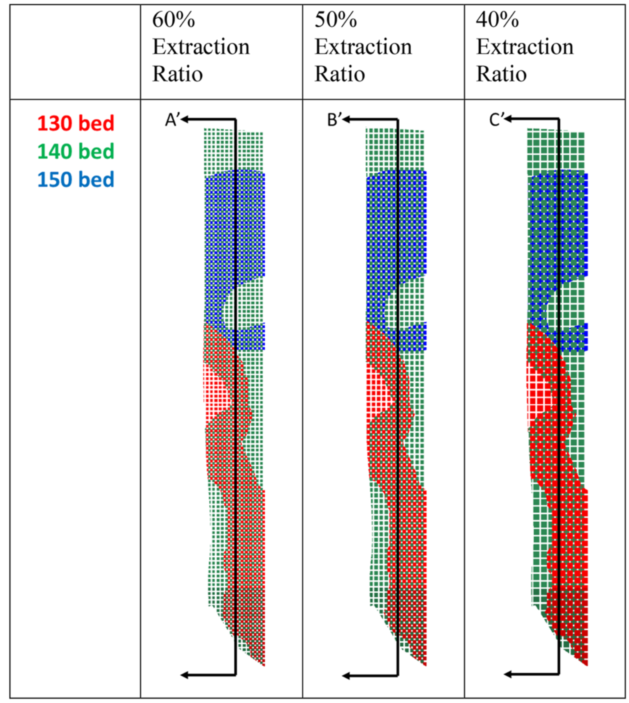

Fig. 13 Staggered pillar configurations evaluated with 60, 50, and 40% extraction ratio

Table 4 Pillar dimensions used in generic mine-wide pillar arrangement for different extraction ratios

Extraction ratio (%)	Pillar width	Pillar length	Mining widths
60	21 m (69 ft)	21 m (69 ft)	12 m (39 ft)
50	30 m (98 ft)	27 m (89 ft)	12 m (39 ft)
40	45 m (148 ft)	45 m (148 ft)	12 m (39 ft)

lower two-thirds of the 140 bed is approximately 65–70 MPa (9427–10,153 psi). This maximum value remains relatively constant due to the also relatively constant depth of cover, while the maximum horizontal shear stress is found toward the down-dip end of the bed and has a maximum magnitude of approximately 27 MPa or 3910 psi (see Fig. 14). This higher horizontal shear concentration corresponds to the steepest part of the orebody, as shown in Fig. 15. The bottom pictures in Fig. 14 show the shear FOS evaluated under the local pillar stress conditions and HR:h ratio using the site-specific design charts in Fig. 10. Several regions in the three different beds show areas, where the resulting shear FOS is less than 1, while some regions, such as the down-dip second half of the 130 bed, exhibit a shear FOS > 2 for the case of rectangular pillars. When rhomboidal pillars were evaluated in the steeply dipping sections of the beds, more extensive regions were identified, where the pillars under the 60% extraction ratio assumption would be compromised; this is the case, because rhomboidal pillars exhibit less resistance to shear than their rectangular counterparts.

The results of the staggered pillar configuration under the 50% extraction ratio are shown in Fig. 16. The lower extraction ratio results in lower average pillar vertical stresses and horizontal shear stresses, which translate into better pillar performance. For the case of rectangular

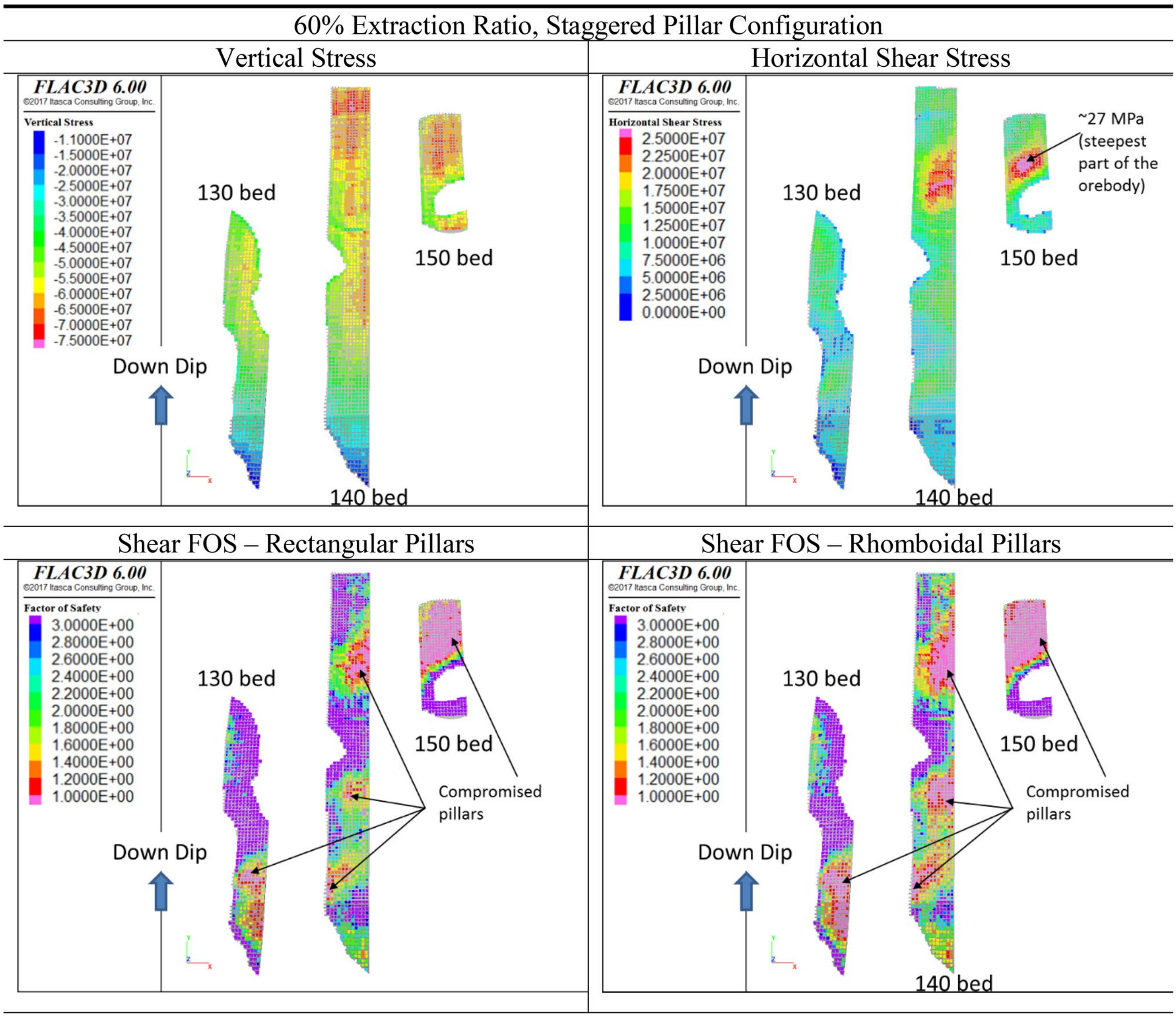

Fig. 14 Average pillar vertical stress and horizontal shear stress distribution (top left and right, respectively) in the mine-wide model with staggered pillar configuration after mining all the beds at Montanore with 60% extraction ratio. The associated shear FOS assuming rectangular pillars (bottom left) and rhomboidal pillars (bottom right) using the design charts in Fig. 10 are also shown

pillars, the shear FOS evaluation suggests that most of the pillars in the 130 and 140 beds would have shear FOS in excess of 1.3, while the steeply dipping section of the 150 bed would still be compromised at this extraction ratio. As before, rectangular pillars exhibit higher shear FOS than their rhomboidal counterparts. However, at this extraction ratio, a large portion of the pillars in the 130 and 140 bed would be stable even with the rhomboidal configuration.

Figure 17 shows the results of the staggered pillar configuration under the 40% extraction ratio. At this extraction ratio, all pillars (including rhomboidal shape) are expected to have a shear FOS > 1.3.

Under the current strength assumptions, FOS > 1.3 could be achieved in the different beds with (assuming right-angled pillars):

- a local extraction ratio ~ 60% for most of the 130 bed with some sections at 50%;
- bed 140 could be mostly mined with an extraction ratio of 60%, with some sections (steeply dipping) at 50%;
- the extraction ratio of bed 150 would need to vary from 60% down to 40% in the steeply dipping sections.

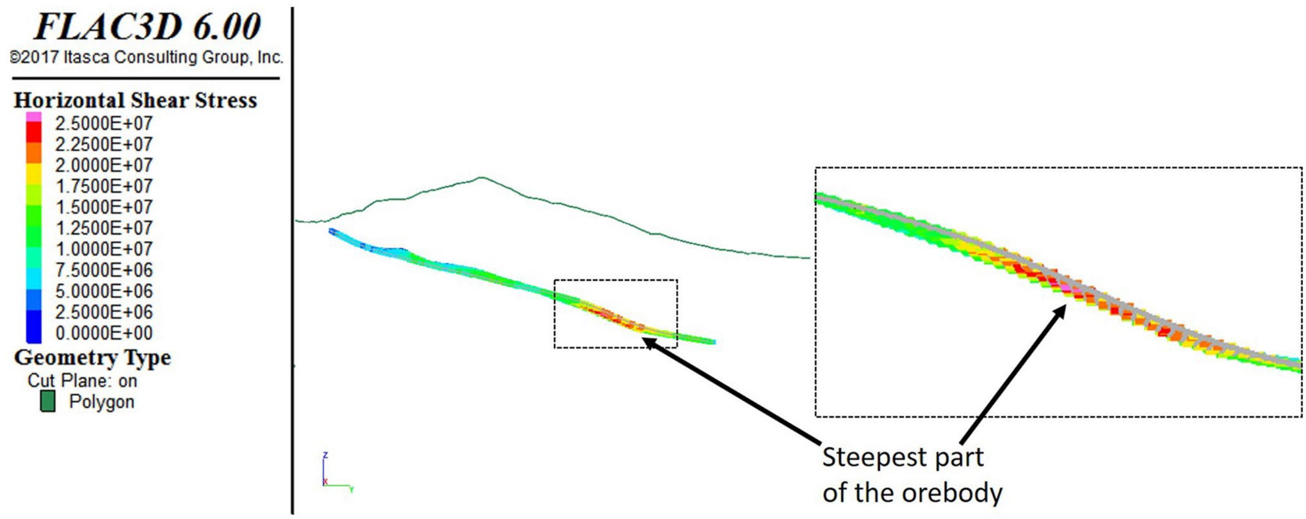

Fig. 15 Horizontal shear stresses on pillars in the 140 bed reach a maximum in the steepest part of the orebody

7 Conclusions

Orebody geometry in relation to topography can lead to significant shear stresses in pillars. A back analysis on the pillar collapses experienced at Troy revealed that the pillars were subject to shear stresses that lowered their capacity, as shear stresses result in significant loss of confinement in pillar core. The use of design methods that do not take into account the detrimental effect of shear stress on pillar capacity may result in under-designed pillars. Analogously, back analysis of failed pillars without taking the shearing effect into account would result in underestimation of the rock mass strength.

The pillar shape affects the effective size of the confined core (loss of confinement near sharp corners), with rhomboidal pillars having smaller confined cores than their rectangular counterparts and, hence, lower capacity. This is because rhomboidal pillars have a smaller hydraulic radius (HR) than a rectangular pillar with an equivalent width and area. The results from this analysis suggest that the use of hydraulic radius provides a better measure of pillar shape than pillar width alone, this aspect is often omitted in pillar design. In addition, the initial level of confinement for a pillar of a given geometry also depends on the local in situ stress level before the pillar is mined; therefore, pillars with a high HR:h ratio would have a larger level of core confinement if they are located deeper in the mine. It is the interplay between pillar demand and pillar strength based on confinement that determines the emergent pillar stability.

Numerical models can greatly aid in the local design and evaluation of pillars within panels under complex loading conditions with variable seam thickness. When designing pillars that are likely to be subjected to shear, keeping the pillar angles as close to 90° as possible would increase its HR and hence its shear capacity.

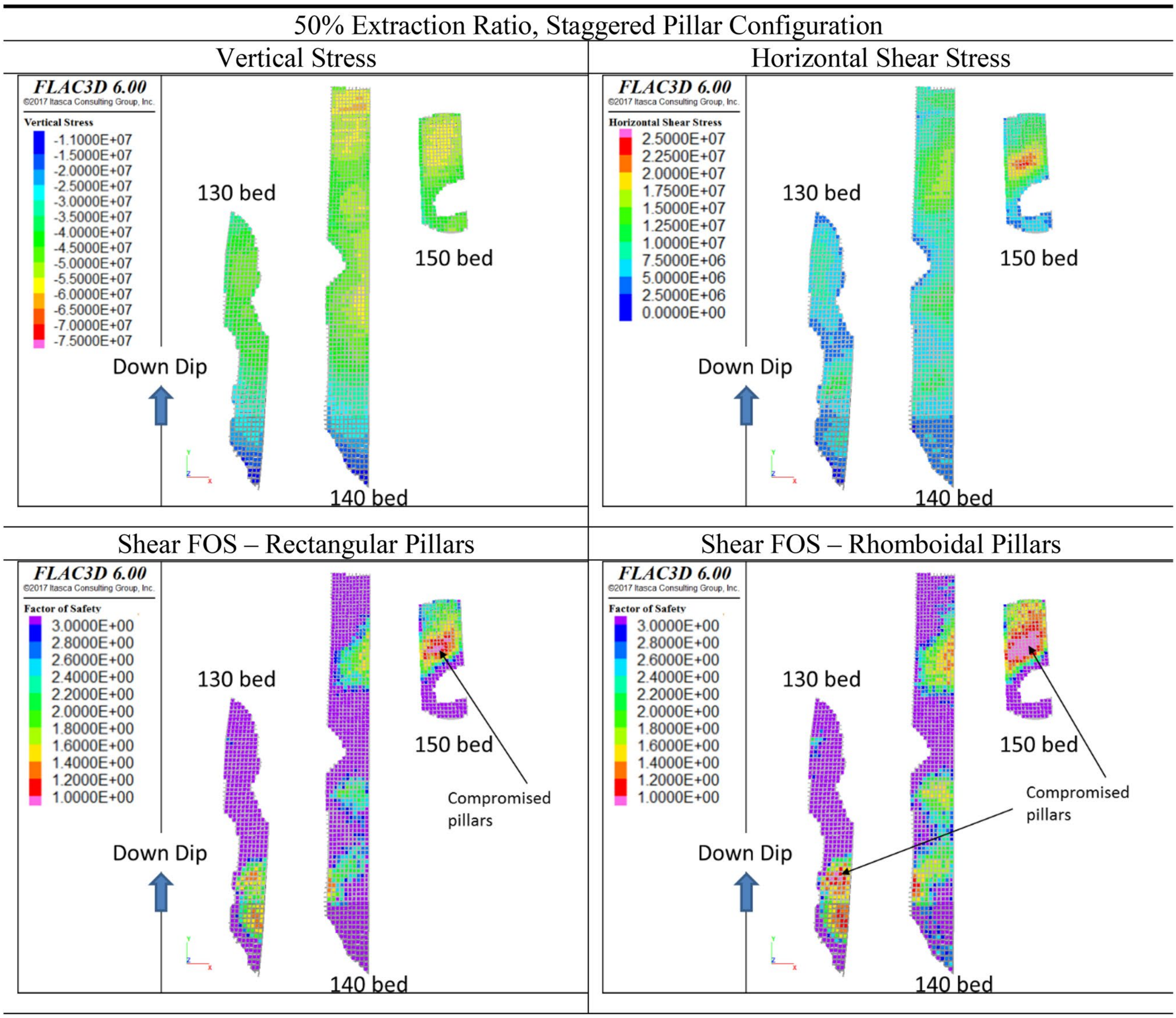

Fig. 16 Average pillar vertical stress and horizontal shear stress distribution (top left and right, respectively) in the mine-wide model with staggered pillar configuration after mining all the beds at Montanore with 50% extraction ratio. The associated shear FOS assuming rectangular pillars (bottom left) and rhomboidal pillars (bottom right) using the design charts in Fig. 10 are also shown

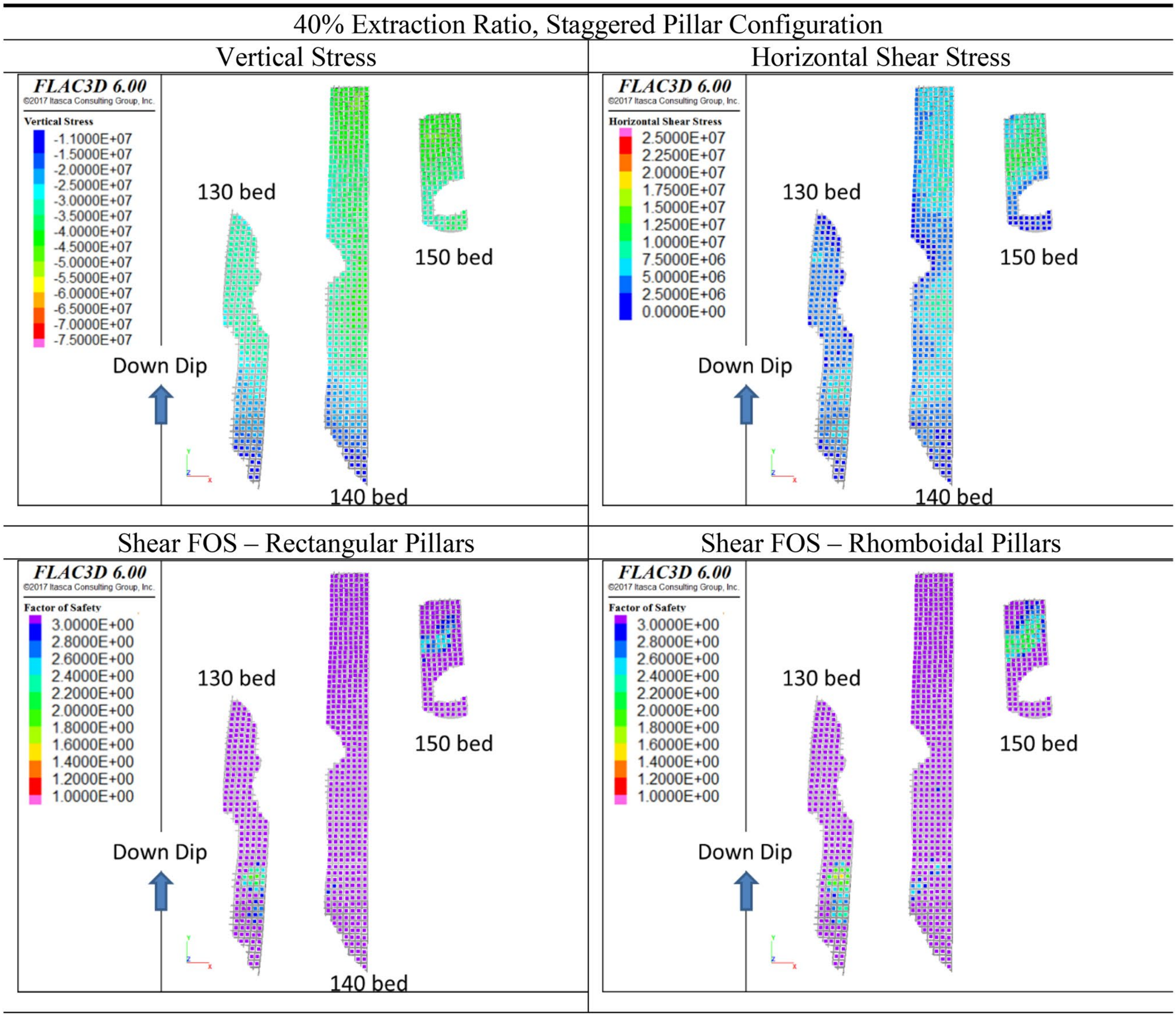

Fig. 17 Average pillar vertical stress and horizontal shear stress distribution (top left and right, respectively) in the mine-wide model with staggered pillar configuration after mining all the beds at Montanore with 40% extraction ratio. The associated shear FOS assuming rectangular pillars (bottom left) and rhomboidal pillars (bottom right) using the design charts in Fig. 10 are also shown

Acknowledgements The authors would like to thank the Hecla Mining Company for permission to publish this paper. The authors also acknowledge the peer reviewers for their suggestions.

References

Beus MJ, Chan SSM (1980) Shaft design in the Coeur d'Alene Mining District, Idaho-results of in situ stress and physical property measurements. BuMines RI 8435, p 39

Board M (2017) Inspection of bedding and jointing in the Lower Revett—Montanore. Hecla Mining Memorandum to Itasca Consulting Group Inc, Coeur d'Alene

Board MP, Beus MJ (1989) In situ measurements and preliminary design analysis for deep mine shafts in highly stressed rock. Report of Investigations RI-9231. U.S. Bureau of Mines

Boleneus DE, Appelgate LM, Stewart JH, Zientek ML (2006) "trata-bound copper-silver deposits of the Mesoproterozoic Revett Formation, Montana and Idaho. Scientific Investigations Report 2005-5231. Reston, Virginia: U.S. Department of the Interior, U.S. Geological Survey

Bowden TD (1977) Depositional processes and environments within the Revett Formation, pre-Cambrian Belt Supergroup, northwestern Montana and northern Idaho. M.S. thesis, University of California, Riverside, p 161

Cicchini PF, Killian JR (2014) Analysis of subsidence and ground fall at the Troy Mine. Prepared for Troy Mine, Inc. by Call & Nicholas, Inc., September 10

Coates DF (1981) Rock mechanics principles. Ottawa: Mines Branch Monograph 874, Information Canada

Damjanac B, Board M, Lin M, Kicker D, Leem J (2007) Mechanical degradation of emplacement drifts at Yucca Mountain—a modeling case study, Part II: lithophysal rock. Int J Rock Mech Min Sci 44:368–399

Esterhuizen GS, Dolinar DR, Ellenberger JL (2008) Assessment of stable and failed pillars in underground limestone mines. Min Eng 61(11):43–48

Garza-Cruz TV, Pierce M (2014) A 3DEC model for heavily veined massive rock masses. In: Proceedings, 48th US rock mechanics/geomechanics symposium (Minneapolis, Minnesota, June 2014), ARMA 14-7660. ARMA, Alexandria, Virginia

Garza-Cruz TV, Pierce M, Kaiser PK (2014) Use of 3DEC to study spalling and deformation associated with tunnelling at depth. In: Deep mining 2014 (proceedings, seventh international conference on deep and high stress mining, Sudbury, Canada, September 2014). Australian Centre for Geomechanics, Perth, pp 421–436

Hayes TS (1983) Geologic studies on the genesis of the Spar Lake stratabound copper-silver deposit, Lincoln County, Montana: Stanford, Calif., Stanford University, Ph.D. Thesis, p 340

Hoek E, Brown ET (1980) Underground excavations in rock. Institution of Mining and Metallurgy London, London

Hoek E, Diederichs MS (2006) Empirical estimates of rock mass modulus. Int J Rock Mech Min Sci 43:203–215

Itasca Consulting Group, Inc. (2014) PFC3D—particle flow code in three dimensions, (Ver. 5). Itasca, Minneapolis

Itasca Consulting Group, Inc. (2016a) 3DEC—three-dimensional distinct element code (Ver. 5.2) Itasca Consulting Group, Inc. Itasca, Minneapolis

Itasca Consulting Group, Inc. (2016b) Griddle™ (Version 1.0). Itasca, Minneapolis

Itasca Consulting Group, Inc. (2017) FLAC3D—fast Lagrangian analysis of continua in three dimensions (Version 6.0). Itasca, Minneapolis

Kaiser P (2016) Ground support for constructability of deep underground excavations. Muir Wood Lecture, presented at World Tunnel Congress (San Francisco, April 2016). Lausanne: ITA/AITES. ISBN 978-2-9701013-8-3

Lan H, Martin D, Hu B (2010) Effect of heterogeneity of brittle rock on micromechanical extensile behavior during compression loading. J Geophys Res. https://doi.org/10.1029/2009JB006496

Langstaff J (1976) Hecla's seismic detection system. Paper in site characterization: 17th US symposium on rock mechanics (Snowbird, UT). Univ. UT, Salt Lake City, UT, pp 3 A7-1–3 A7-20

Martin CD, Maybee WG (2000) The strength of hard-rock pillars. Int J Rock Mech Min Sci 37:1239–1246

Mgumbwa JJ (2011) Failure mechanisms of orebodies under shear loading. MSc thesis, Laurentian University, Sudbury, Ont., Canada

Noranda and Call and Nicholas (1989) Preliminary rock mechanics study of the Montanore Project. Noranda Technology Center Geomechanics Group and Call & Nicholas, Inc., Report

Pariseau WG (1982) Shear stability of mine pillars in dipping seams. In Goodman RE, Heuze FE (eds) Issues in rock mechanics. NY: SME, pp 1077–1090

Suorineni FT, Kaiser PK, Mgumbwa JJ, Thibodeau D (2011) Mining of orebodies under shear loading Part 1—case histories. Trans Inst Min Metall Sect A Min Technol 120(3):137–147

Suorineni FT, Kaiser PK, Mgumbwa JJ, Thibodeau D (2014) Mining of orebodies under shear loading Part 2—failure modes and mechanisms. Trans Inst Min Metall Sect A Min Technol 123(4):240–249

Tetra Tech, Inc. and R Squared Incorporated (2006) Final geotechnical assessment report sinkhole development at the Troy Mine and implications for the proposed rock creek mine, Lincoln and Sanders Counties, Montana. Report to Forest Supervisor, Kootenai National Forest, USDA Forest Service Region 1, June 15, p 44

United States Forest Service (FS) and Montana Department of Environmental Quality (MDEQ) (2001) Rock creek final environmental impact statement, September